Partially-Shared Variational Auto-encoders for Unsupervised Domain Adaptation with Target Shift

Ryuhei Takahashi
Kyoto University
takahashi@mm.media.kyoto-u.ac.jp

Atsushi Hashimoto
OMRON SINIC X Corp.
atsushi.hashimoto@sinicx.com

Motoharu Sonogashira
Kyoto University
sonogashira@mm.media.kyoto-u.ac.jp

Masaaki Iiyama
Kyoto University
iiymama@mm.media.kyoto-u.ac.jp

Abstract

This paper proposes a novel approach for unsupervised domain adaptation (UDA) with target shift. Target shift is a problem of mismatch in label distribution between source and target domains. Typically it appears as class-imbalance in target domain. In practice, this is an important problem in UDA; as we do not know labels in target domain datasets, we do not know whether or not its distribution is identical to that in the source domain dataset. Many traditional approaches achieve UDA with distribution matching by minimizing mean maximum discrepancy or adversarial training; however these approaches implicitly assume a coincidence in the distributions and do not work under situations with target shift. Some recent UDA approaches focus on class boundary and some of them are robust to target shift, but they are only applicable to classification and not to regression.

To overcome the target shift problem in UDA, the proposed method, partially shared variational autoencoders (PS-VAEs), uses pair-wise feature alignment instead of feature distribution matching. PS-VAEs inter-convert domain of each sample by a CycleGAN-based architecture while preserving its label-related content. To evaluate the performance of PS-VAEs, we carried out two experiments: UDA with class-unbalanced digits datasets (classification), and UDA from synthesized data to real observation in human-pose-estimation (regression). The proposed method presented its robustness against the class-imbalance in the classification task, and outperformed the other methods in the regression task with a large margin.

1. Introduction

Unsupervised domain adaptation (UDA) is one of the most studied topics in recent years. One attractive application of UDA is adaptation from computer graphic (CG)
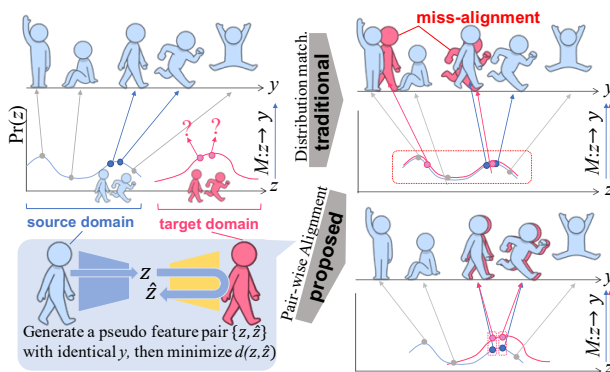

Figure 1. (best viewed in color) Overview of the proposed approach. When two domains have different label distributions, feature distribution matching causes miss-alignment in feature space (with classifier/regressor $M : z \rightarrow y$ trained by source domain samples). The proposed method avoids this by sample-wise feature matching, where pseudo sample pairs with identical label are generated via a CycleGAN-based architecture.

data to sensor-observed (Obs.) data. By constructing a CG-rendering system, we can easily obtain a large amount of supervised data with diversity for training. We denote this task as CG→Obs. UDA is typically tested on semantic segmentation of traffic scenes [11, 32] and achieves remarkable performance.

As in ADDA[36], the typical approach for UDA is to match feature distributions between the source and target domains [21, 8, 18]. This approach works impressively with balanced datasets, such as those for digits (MNIST, USPS, and SVHN) and traffic-scene semantic-segmentation (GTA5[28]→cityscapes[5]). When the prior label distributions of the source and target domains are mismatched, however, such approaches hardly work without a counter-measure for the mismatch (see Figure 1). Cluster finding [32, 31, 6] is another approach for UDA, and such ap-

proaches are more robust against cases of mismatched distributions; they are not, however, applicable to regression problems.

In this paper, we propose a novel UDA method applicable to both classification and regression problems with mismatched label distributions. The problem of mismatched label distributions is also known as target shift [39, 10] or prior probability shift [26]. The typical example of this problem is hidden class-imbalance in the target domain dataset. Previous methods on deep learning models tried to overcome this problem by estimating importance labels for each category [37, 38, 1, 2, 3] or each sample [14]. The former approach is only applicable to classification tasks, while the latter under-samples the source domain data.

In contrast, our method resolves this problem by oversampling with data augmentation via the CycleGAN architecture [41]. More concretely, the basic strategy of the method is to generate pseudo-pairs of source and target samples (with identical labels) by using the CycleGAN architecture. Unlike other CycleGAN-based UDA methods [11, 30], the proposed method does not match feature distributions. Instead, it aligns features extracted from each pseudo-pair in feature space as shown in Figure 1. In addition, the two encoders are designed to share weights. The same encoder is used in encoding any sample of the pseudo-pair. Naively minimizing distance between the paired samples leads to bad convergence because of the competition with the losses in CycleGAN training; it implicitly forces features on the source→target and target→source paths to contain different information in addition to the common label-related content. Hence, we disentangle the features into domain-invariant and domain-specific components to avoid such competition. We further stabilize training by making the encoders and decoders share weights, giving what we call partially-shared autoencoders (PS-AEs). As a side benefit, this implementation enables us to introduce the mechanism of a variational auto-encoder (VAE) [7], which is known to be effective for DA tasks [18, 20].

The contribution of this paper is three-fold.

- We propose a novel UDA method that overcomes the target shift problem by oversampling with data augmentation.

- The proposed method achieved the best performance for UDA with heavily-class-imbalanced digit datasets.

- We tackled the problem of human-pose estimation by UDA with target shift for the first time and outperformed the baselines with a large margin.

2. Related Work

The most popular approach in recent UDA methods is to match the feature distributions of the source and target

Table 1. Representative UDA methods and their supporting situations. The symbol "(✓)" indicates that the method theoretically supports the situation but this was not experimentally confirmed in the original paper. The abbreviations "cat." and "reg." indicate categorization and regression, respectively.

	Balance		Imbalance	
	cat.	reg.	cat.	reg.
ADDA [36], UFDN [18], CyCADA [11]	✓	(✓)		
MCD [32]	✓		(✓)	
PADA [37]	(✓)		✓	
SimGAN [33]		✓		(✓)
Ours	✓	(✓)	✓	✓

domains so that a classifier trained with the source domain dataset is applicable to target domain samples. There are various options to match the distributions, such as minimizing MMD [21, 37], using a gradient-reversal layer with domain discriminators [8], and using alternative adversarial training with domain discriminators [36, 15, 2, 18]. Adversarial training removes domain bias from the feature representation. To preserve information in features as much as possible, UFDN [18] adds a decoder to the network for a loss-less encoding. Because the features have no domain information, this method feeds a domain code, a one-hot vector representation for domain reference, to the decoder (with the encoded feature). The encoder and decoder in this model compose a VAE [7]. Another approach is feature whitening [29], which whitens features from each domain at domain-specific alignment layers. This approach does not use adversarial training, but it tries to analytically fit a feature distribution from each domain to a common spherical distribution. As shown in Table 1, all these methods are theoretically applicable to both classification and regression, but it is limited to the situations without target shift.

MCD was proposed by Saito *et al.* [32, 31], which does not use distribution matching. Instead, the classifier discrepancy is measured based on the difference of decision boundaries between multiple classifiers. DIRT-T [34] and CLAN [22] are additional approaches focusing on boundary adjustment. These approaches are expected to be robust against class imbalance, because they focus only on the boundaries and do not try to match the distributions. CAT [6] is a method that aligns clusters found by other backbone methods. These approaches assume an existence of boundaries between clusters. Hence, they are not applicable to regression problems, which have continuous sample distributions (see the second row in Table 1).

Partial domain adaptation (PDA) is a variant of UDA with several papers on it [37, 38, 1, 2, 3] (see the third row in Table 1). This problem assumes a situation in which some categories in the source domain do not appear in the target domain. This problem is a special case of UDA with target shift in two senses: it always assumes the absence of a

class rather than class-imbalance, and it does not assume a regression task. The principle approach for this problem is to estimate the importance weight for each category, and ignore those judged as unimportant (under-sampling). PADACO [14] is an extension of PADA for a regression problem and was designed to estimate head poses in UDA with target shift. It first trains the model with the source domain dataset and obtains pseudo-labels for the target domain dataset. Then, using the similarity of estimated labels, it sets a sampling weight for each sample in the source domain (under-sampling). Finally, it performs UDA training with a weighted sampling strategy for the source domain dataset. To obtain better results with this method, it is important to obtain good sampling weights at the first stage. In this sense, like CAT [6], PADACO requires a good backbone method that provides a good label similarity metric.

Label-preserving domain conversion is another important approach and includes the proposed method (see fourth and fifth rows in Table 1). Shrivastava *et al.* proposed SimGAN [33], which converts CG images to nearly real images by adversarial training. This method tries to preserve labels by minimizing the self-regularization loss, the pixel-value difference between images before and after conversion. In the sense that the method generates source-domain-like samples from the source domain datasets using GAN, we can say it is a method based on over-sampling with data augmentation. We note that this work can be regarded as the first deep-learning-based UDA method for regression that is theoretically applicable to the task with target shift.

CyCADA[11] combines CycleGAN, ADDA and SimGAN for better performance. It first generates fake target domain images via CycleGAN. The label-consistency of generated samples are preserved by SimGAN's self-regularization loss; however it has a discriminator that matches the feature distributions. Hence, this methods principally has the same weakness against target shift. SBADAGAN[30] is yet another CycleGAN-based method with discriminator for feature distribution matching.

From the viewpoint of human-pose-estimation, a method has been proposed quite recently that estimates human-pose in a UDA manner [40]. It uses a synthesized depth image dataset as the source domain dataset. The target domain is given with depth and RGB images. The final goal is to estimate 3D poses from RGB images. It performs domain adaptation by transferring knowledge via an additional domain of body-part label representations. The body-part label space are expected to be domain-invariant because of its discrete representation. The method tries to transfer knowledge through this discrete space. The method was evaluated in UDA, weakly-supervised DA, and fully supervised DA settings. Target shift was not discussed in this paper because the target domain dataset has enough diversity.

3. Method

3.1. Problem statement

Let $\{x_s, y_s\} \in X_s \times L$ be samples and their labels in the source domain dataset (L is the label space), and let $x_t \in X_t$ be samples in the target domain dataset. The target labels Y_t and their distribution $\Pr(Y_t)$ are unknown (and shiftable from $\Pr(Y_s)$) in the problem of UDA with target shift. The goal of this problem is to obtain a high-accuracy model for predicting the labels of samples obtained in the target domain.

3.2. Overview of the proposed method

The main strategy of the proposed method is to replace the feature distribution matching process with pair-wise feature alignment. To achieve this, we adopt the CycleGAN architecture shown in Figure 2. The model is designed to generate pseudo pairs $(x_s, \hat{x}_t)$ and $(x_t, \hat{x}_s)$, each of which are expected to have an identical label. In addition to CycleGAN's original losses, we add two new losses: L_{pred} for label prediction and L_{fc} for feature alignment, where the losses are calculated only on the domain-invariant component z of the disentangled feature representation z_s (or z_t). After the training, prediction in target domain is done by the path, encoder→predictor ($M \circ E_t$). 3.3 describes this modification in detail.

To preserve the label-related content at pseudo pair generation, we further modify the network by sharing weights and introducing VAE's mechanism (see Figure 3). 3.4 describes this modification in detail.

3.3. Disentangled CycleGAN with feature consistency loss

The model in Figure 2 has pairs of encoders E_*, generators G_*, and discriminators D_*, where $* \in \{s, t\}$. $\hat{x}_t$ is generated as $\hat{x}_t = G_t(E_s(x_s))$, and $\hat{x}_s$ as $\hat{x}_s = G_s(E_t(x_t))$. The original CycleGAN [41] is trained by minimizing the cycle consistency loss L_{cyc}, the identity loss L_{id}, and the adversarial loss L_{adv} defined in LSGAN [24]:

$$\min_{E_s, E_t, G_s, G_t} L_{cyc}(X_s, X_t) = \sum_{* \in \{s,t\}} \mathbb{E}_{x \in X_*}[d(x, G_*(E_{\bar{*}}(\hat{x}_{\bar{*}})))], \quad (1)$$

where $\bar{*}$ is the opposite domain of $*$ and d is a distance function.

$$\min_{E_s, E_t, G_s, G_t} L_{id}(X_s, X_t) = \sum_{* \in \{s,t\}} \mathbb{E}_{x \in X_*}[d(x, G_*(E_*(x)))]$$

$$\min_{E_s, E_t, G_s, G_t} \max_{D_s, D_t} L_{adv}(X_s, X_t) = \mathbb{E}_{\{x_s, x_t\} \in X_s \times X_t} \quad (2)$$

$$[\|D_s(x_s) - 1\|_2 + \|D_s(G_s(E_t(x_t))) + 1\|_2 \quad (3)$$
$$+ \|D_t(x_t) - 1\|_2 + \|D_t(G_t(E_s(x_s))) + 1\|_2]$$

We note that we used spectral normalization [25] in D_s and D_t for a stable adversarial training.
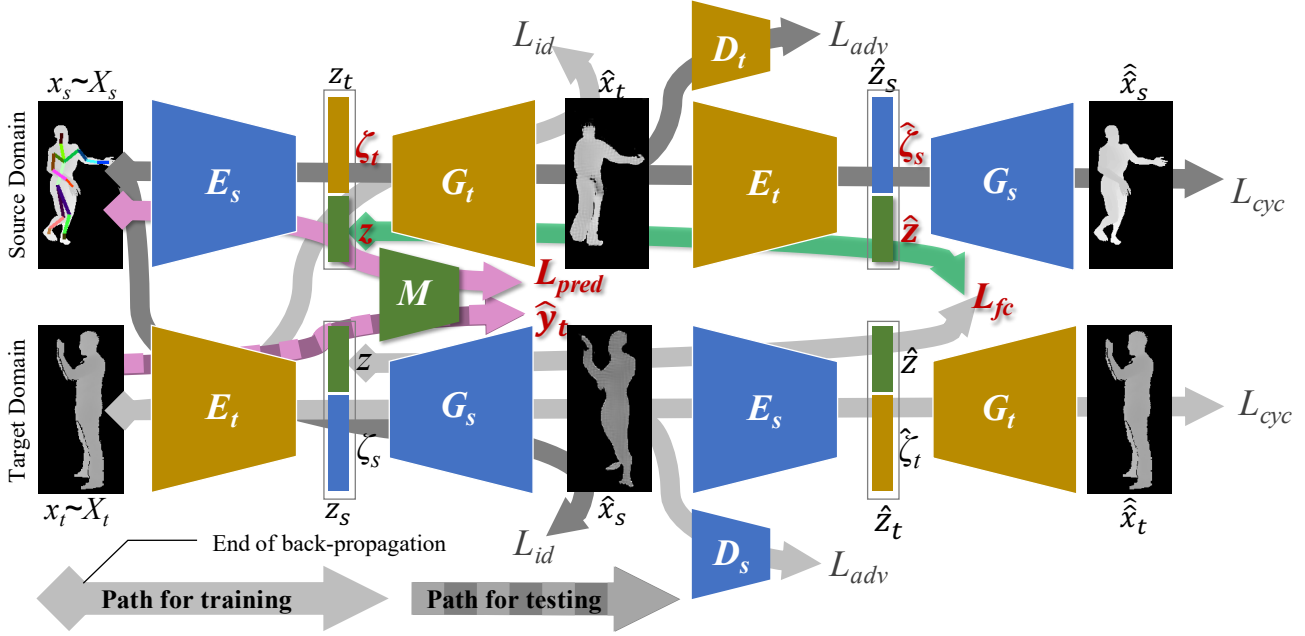
Figure 2. (best viewed in color) Architecture of CycleGAN with disentangled features. The major changes from the original CycleGAN (variables, losses with their back-propagating paths) are shown in color.
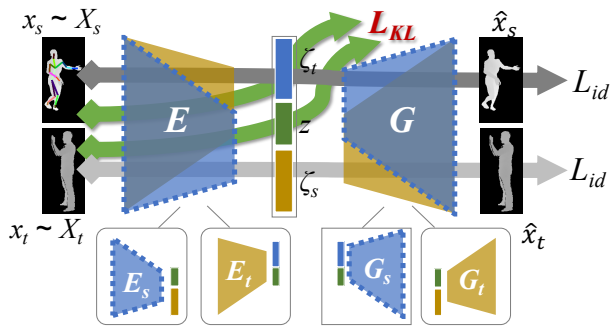

Figure 3. (best viewed in color) Architecture of partially-shared variational auto-encoders $\hat{x}_s = G_s(E_t(x_s))$ and $\hat{x}_t = G_t(E_s(x_t))$ with the path for calculating L_{id}. VAE's re-sampling process is applied when calculating L_{id} but not with other losses.

Figure 4. Misalignment caused by CycleGAN's two image-space discriminators. This is typically seen with a model that does not share encoder weights.

To successfully achieve pair-wise feature alignment, the model divides the output of E_* into $z_{\bar{*}} = \{z, \zeta_{\bar{*}}\}$. Then, it performs feature alignment by using the domain-invariant feature consistency loss L_{fc}, defined as

$$\min_{E_s, E_t, G_s, G_t} L_{fc}(Z_s, Z_t) = \sum_{*\in\{s,t\}} \mathbb{E}_{z\in Z_*}[d(z, E_{\bar{*}}(G_{\bar{*}}(z)))], \quad (4)$$

where $Z_* = E_*(X_*)$. Note that gradients are not further back-propagated to E_* over z (see the path of L_{fc} in Figure 2) because updating both z and $\hat{z}$ in one step leads to bad convergence.

In addition, z obtained from x_s is fed into M to train the classifier/regressor $M : z \rightarrow \hat{y}$ by minimizing the prediction loss $L_{pred}(X_s, Y_s)$. The concrete implementation of
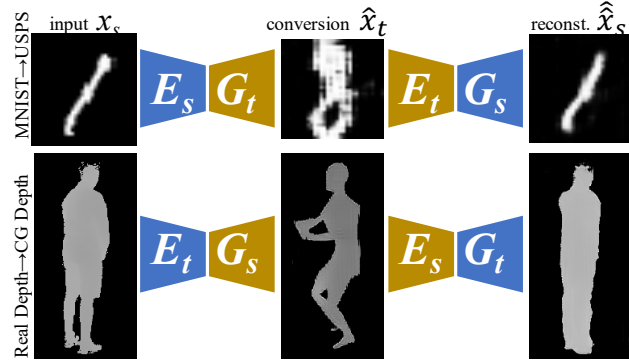
L_{pred} is task-dependent.

We avoid applying L_{fc} to the whole feature components z_t, as it can hardly reach good local minima because of the competition between the pair-wise feature alignment (by L_{fc}) and CycleGAN (by L_{cyc} and L_{id}). Specifically, training G_t to generate $\hat{x}_t$ must yield a dependency of $\text{Pr}(z_t|x_t)$. This means that $\hat{z}_t$ is trained to have in-domain variation information for x_t. The situation is the same with x_s and z_s. Hence, $\hat{z}_t$ and $\hat{z}_s$ have dependencies on different factors, x_t and x_s, respectively, and it is difficult to match the whole features, $\hat{z}_t$ and $\hat{z}_s$. The disentanglement into z and ζ_* resolves this situation. Note that this architecture is similar to DRIT [17].

3.4. Partially shared VAEs

Next, we expect E_s and E_t to output a domain-invariant feature z. Even with this implementation, however, CycleGAN can misalign an image's label-related content in domain conversions under a severe target shift, because it has discriminators that match not feature- but image-distributions. Figure 4 shows examples of misalignment caused by image space discriminators. This happens because the decoders G_s and G_t can convert identical zs into different digits, for example, to better minimize L_{adv} with imbalanced distributions. In such cases, the corresponding encoders also extract identical zs from images with totally different appearance.

To prevent such misalignment and get more stable results, we make the decoders share weights to generate similar content from z, and we make the encoders extract z only from similar content. Figure 3 shows the details of the parameter-sharing architecture, which consists of units called *partially-shared auto -encoders* (PS-AEs). Formally, the partially shared encoders are described as a function $E : x \rightarrow \{z, \zeta_s, \zeta_t\}$. In our implementation, only the last layer is divided into three parts, which outputs z, ζ_s, and ζ_t. E can obviously be substituted for E_s and E_t by discarding ζ_t and ζ_s from the output, respectively. Similarly, the generator $G : \{z, \zeta_s, \zeta_t\} \rightarrow \hat{x}$ shares weights other than for the first layer, which consists of three parts, which output z, ζ_s, and ζ_t. G can be substituted for G_s and G_t by inputting $\{z, \zeta_s, \mathbf{0}\}$ and $\{z, \mathbf{0}, \zeta_t\}$, respectively.

This implementation brings another advantage for UDA tasks: it can disentangle the feature space by consisting of two variational auto-encoders (VAEs), $G_s \circ E_t$ and $G_t \circ E_s$ (Figure 3). Putting VAE in a model to obtain a domain-invariant feature is reported as an effective option in recent domain adaptation studies [18, 20]. To make PS-AEs a pair of VAEs, we put VAE's resampling process at calculation of L_{id} and add the KL loss defined as

$$\min_{E_s, E_t} L_{KL}(X_s, X_t) = \sum_{* \in \{s,t\}} \mathbb{E}_{z, \zeta_* \in E_*(X_*)}[KL(p_z|q_z) + KL(p_{\zeta_*}|q_{\zeta_*})], \quad (5)$$

where $KL(p\|q)$ is the KL divergence between two distributions p and q, p_{ζ_*} is the distribution of ζ_* sampled from X_*, and q_z and q_{ζ_*} are standard normal distributions with the same sizes as z and ζ_*, respectively.

Our full model, *partially-shared variational auto-encoders* (PS-VAEs), is trained by optimizing the weighted sum of the all the above loss functions:

$$L_{total} = L_{adv} + \alpha L_{cyc} + \beta L_{id} + \gamma L_{KL} + \delta L_{fc} + \epsilon L_{pred}, \quad (6)$$

where α, β, γ, δ, and ϵ are hyper-parameters that should be tuned for each task. For the distance function d, we use the

Table 2. Number of samples under each condition. SVHN was only used as a source domain and had no imbalanced setting.

	10%	20%	30%	40%	50%
USPS (1)	500	1125	1922	3000	4500
USPS (other)	500	500	500	500	500
MNIST (1)	4000	4500	5400	6000	6300
MNIST (other)	4000	2000	1400	1000	700
SVHN (1)	4000	-	-	-	-
SVHN (other)	4000	-	-	-	-

smooth L1 distance [9], which is defined as

$$d(a, b) = \begin{cases} \|a - b\|_2 & \text{if } |a - b| < 1 \\ |a - b| - 0.5 & \text{otherwise} \end{cases} \quad (7)$$

4. Evaluation

4.1. Evaluation on class-imbalanced digit dataset

We first evaluated the performance of the proposed method on standard UDA tasks with digit datasets (MNIST[16]↔USPS[12], and SVHN[27]→MNIST). To evaluate the performance under a controlled situation with class-imbalance in the target domain, we adjusted the rate of samples of class '1' from 10% to 50%. When the rate was 10%, the number of samples was exactly the same among the categories. When it was 50%, half the data belonged to category '1,' which was the most imbalanced setting in this experiment. Note that the original data had slight differences in the numbers of samples between categories. We adjusted these differences by randomly eliminating samples. Table 4.1 lists the numbers of samples in each dataset and class-imbalance. Because SVHN was used only as a source domain, it had no imbalanced situation. Note that USPS had only small numbers of samples (500 to 1000 for each category). Hence, we over-sampled data from category '1' with data augmentation (horizontal shifts of one or two pixels) to achieve the balance. For the other datasets, we randomly discarded the samples.

In this task, L_{pred} is simply given as the following categorical cross-entropy loss:

$$\min_{E_s, M} L_{pred}(Y_s, X_s) = \mathbb{E}_{x_s, y_s \in X_s \times L}[-y_s \log M(E(x_s))] \quad (8)$$

We compared the proposed method with the following baselines:

ADDA[36] and UFDN[18] are methods based on simple distribution matching. They are applicable to both classification and regression.

PADA[2] is also based on distribution matching, but it estimates an importance weight for each category to deal with class-imbalance.

SimGAN[33] is a method based on image-to-image conversion. To prevent misalignment during conversion,

Table 3. Accuracy in the MNIST→USPS task. The abbreviation "Ref." indicates reference scores reported in the original papers.

	Ref.	10%	20%	30%	40%	50%
Source only	-	71.0	-	-	-	-
ADDA	89.4	89.8	86.9	79.3	81.8	78.5
UFDN	97.1	**94.0**	90.4	83.2	82.3	83.8
PADA	-	75.3	77.7	79.3	77.8	80.2
SimGAN	-	72.4	86.5	84.0	84.3	76.3
CyCADA	95.6	91.8	91.0	80.3	86.4	87.6
MCD	94.2	91.2	90.4	79.0	78.5	80.3
Ours	-	93.9	**94.8**	**93.4**	**94.6**	**92.6**

Table 4. Accuracy in the USPS→MNIST task. The abbreviation "Ref." indicates reference scores reported in the original papers.

	Ref.	10%	20%	30%	40%	50%
Source only	-	55.6	-	-	-	-
ADDA	90.1	**96.0**	89.0	81.5	78.9	80.5
UFDN	93.7	93.6	81.9	79.2	72.0	69.1
PADA	-	47.9	39.2	36.0	29.8	25.2
SimGAN	-	68.3	50.2	49.9	63.8	49.3
CyCADA	96.5	75.3	75.3	75.2	76.7	70.7
MCD	94.1	**96.0**	81.5	79.1	78.1	77.4
Ours	-	94.8	**94.4**	**90.8**	**82.6**	**82.4**

Table 5. Accuracy in the SVHN→MNIST task. The abbreviation "Ref." indicates reference scores reported in the original papers.

	Ref.	10%	20%	30%	40%	50%
Source only	-	46.6	-	-	-	-
ADDA	76.0	75.5	65.0	65.2	50.8	54.3
UFDN	95.0	91.1	70.9	58.7	52.6	43.6
PADA	-	30.5	39.5	37.3	36.8	36.7
SimGAN	-	61.4	52.5	57.7	51.8	49.3
CyCADA	90.4	**91.4**	75.4	69.7	70.7	68.3
MCD	96.2	90.3	**89.7**	**80.2**	**72.0**	65.3
Ours	-	73.7	72.9	73.8	64.4	**68.4**

it also minimizes changes in the pixel-values before and after conversion by using a self-regularization loss. The code is borrowed from the implementation of Cy-CADA.

- **CyCADA[11]** is a CycleGAN-based UDA method. The self-regularization loss is used in this method, too. In addition, it matches feature distributions, like ADDA.

- **MCD[32]** is a method that minimizes a discrepancy defined by the boundary differences obtained from multiple classifiers. This method is expected to be more robust against class-imbalance than methods based on distribution matching, because it does not focus on the entire distribution shape. On the other hand, this kind of approach is theoretically applicable only to classification but not to regression.

Note that some of recent state-of-the-art methods for the balanced digit UDA task was not listed in the experiment due to their reproducibility problem.[1] The detailed implementations (network architecture, hyper-parameters, and so on) of the proposed method and the above methods appears in the supplementary material. Tables 3,4, and 5 list the results. The methods based on distribution matching (ADDA and UFDN) were critically affected by class-imbalance in the target domain. CyCADA was more robust than ADDA and UFDN for the MNIST↔USPS tasks, owing to the self-regulation loss, but it did not work for the SVHN→MNIST task because of the large pixel-value differences between the MNIST and SVHN samples. In contrast, the proposed method was more robust against imbalance than the above methods, and it was more accurate than PADA and Sim-GAN. As a result, our method achieved the best performance in most imbalance settings, and listed its robustness especially with the heaviest imbalance.

4.2. Evaluation on human pose dataset

We also evaluated the proposed method with a regression task on human pose estimation. For this task, we prepared

a synthesized depth image dataset whose poses were sampled with CMU Mocap [4] and rendered with PoserPro2014 [35], as the source domain dataset. Each image had 18 joint positions. In the sampling, we avoided pose duplication by confirming that at least one joint had a position more than 50mm away from its position in any other samples. The total number of source domain samples was 15000. These were rendered with a choice of two human models (male and female), whose heights were sampled from a normal distribution with respective means of 1.707 and 1.579m and standard deviations of 56.0mm and 53.3mm). For the target dataset, we used depth images from the CMU Panoptic Dataset [13], which were observed with a Microsoft Kinect. We automatically eliminated the background in the target domain data by preprocessing.[2] Finally, we used 15,000 images were used for training and 500 images were used for the test, after manually annotating the joint positions.

Figure 5 shows the target shift between the source and target domains via the differences in joint positions at the head and foot. In this experiment, we compared the proposed method with SimGAN, CyCADA, and MCD, with an ablation study. All the methods were implemented with a common network structure, which appears in the supplementary materials. L_{pred} was defined as

$$\min_{E_s,M} L_{pred}(Y_s, X_s) = \mathbb{E}_{x_s, y_s \in \{X_s, Y_s\}}(d(M(E_s(x_s)), y_s)).$$

(9)

---

[1] The authors of [29] provide no implementation and there are currently no other authorized implementations. Two SBADAGAN[30] implementations were available but it was difficult to customize them for this test and the reported accuracy was not reproducible.

[2] The details of this background subtraction appears in the supplementary material.

Table 6. Accuracy in human-pose estimation by UDA (higher is better). Results were averaged for joints with left and right entries (e.g., the "Shoulder" column lists the average scores for the left and right shoulders). The "Avg." column lists the average scores over all samples, rather than only the joints appearing in this table.

| Error less than 10px.	Head	Neck	Chest	Waist	Shoulder	Elbow	Wrists	Hands	Knees	Ankles	Foots	Avg.
Source only	0.4	3.6	1.2	0.4	1.0	2.8	1.0	2.8	1.0	2.6	2.3	1.8
MCD	4.6	7.0	0.2	0.6	1.4	0.2	0.3	0.9	0.4	21.0	16.6	5.3
SimGAN	90.2	68.0	10.8	22.6	38.8	26.3	28.5	33.6	35.9	52.5	52.8	40.4
CyCADA	90.0	69.0	15.4	28.2	39.5	27.3	31.3	32.5	35.4	54.4	53.2	41.0
Ours												
CycleGAN+L_{fc}	82.8	79.0	33.8	17.0	40.0	16.4	15.8	28.4	13.8	51.0	51.5	35.5
D-CycleGAN	**93.0**	**85.8**	21.4	**47.8**	42.5	42.5	35.8	39.2	42.5	66.9	64.1	50.8
D-CycleGAN+VAE	40.6	34.2	17.6	41.2	10.1	10.2	7.5	6.4	20.0	28.0	20.2	18.6
PS-AEs	80.6	72.4	**40.8**	28.0	46.5	28.4	25.2	29.4	25.3	58.9	53.9	42.1
PS-VAEs(full model)	89.4	84.6	21.4	43.4	**51.7**	**54.4**	**49.4**	**43.9**	45.6	**74.5**	**74.0**	**57.0**
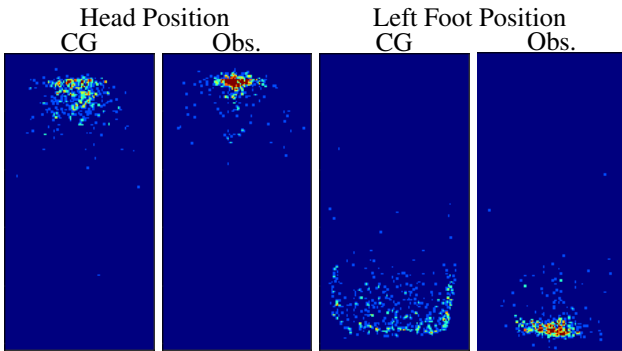
Figure 5. Difference in human joint distributions between the source (CG) and target (Obs.) domains. CG images are generated with diverse poses. In contrast, observed images tend to be stagnation.
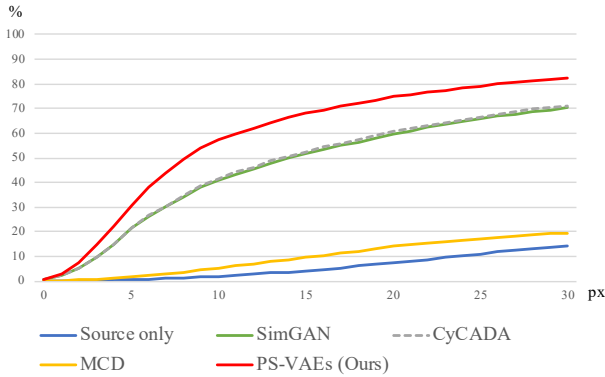

Figure 6. (best viewed in color) Averaged percentage of joints detected with errors less than N pixels. (Higher is better.)

Figure 6 shows the rate of samples whose estimated joint position error is less than thresholds (the horizontal axis shows the threshold in pixels). Table 6 lists the joint-wise results in terms of the rate with threshold of ten pixels. The full model using the proposed methods achieved the best scores on average and for all the joints other than the head, neck, chest, and waist. These four joints have less target shift than others do (see Figure 5, for example). Sim-GAN was originally designed for a similar task (gaze es-
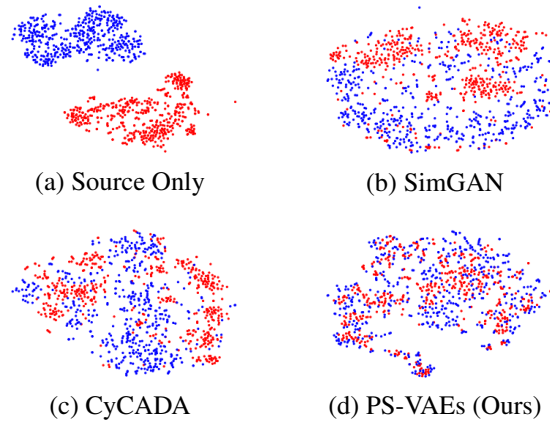

Figure 7. (best viewed in color) Feature distribution visualized by t-SNE [23]: source domain CG data (blue points) and target domain observed data (red points).

timation and hand-pose estimation) and achieved relatively good scores. CyCADA is an extension of SimGAN and has additional losses for distribution matching, but it did not boost the accuracy in the tasks of UDA with target shift. MCD was originally designed for classification tasks and did not work for this regression task, as expected. Figure 7 shows the feature distributions obtained from four different methods. Because SimGAN does not have any mechanisms to align features in the feature space, the distributions did not merge well. CyCADA better mix the distributions, but still the components are separated. In contrast, the proposed method merged features quite well despite no discriminators or discrepancy minimization was performed. This indicates that the proposed pair-wise feature alignment by L_{fc} worked well with this UDA task.

A qualitative difference in domain conversion is shown in Figure 8. SimGAN's self-regularization loss worked to keep the silhouette of generated samples, but subtle depth differences in the body regions were not reproduced well. In contrast, the proposed method seems to be able to reproduce such subtle depth differences with the silhouette. This
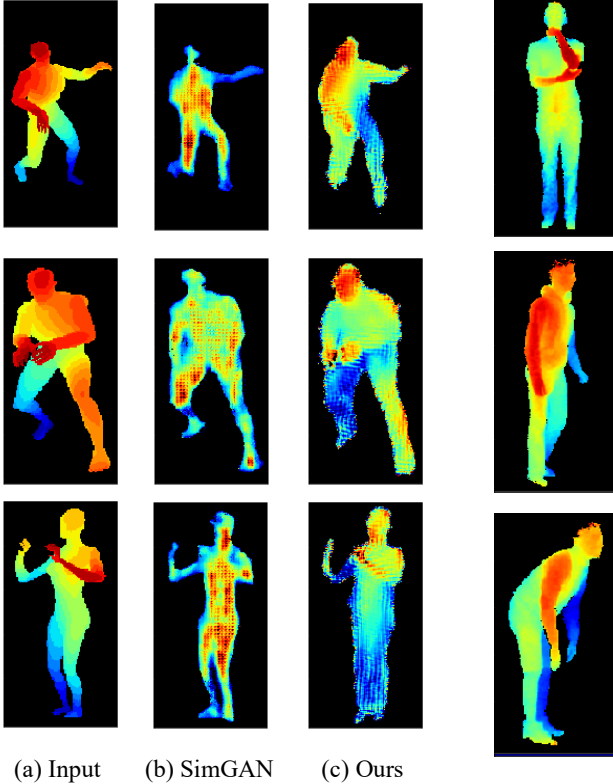
(a) Input   (b) SimGAN   (c) Ours

Figure 8. (best viewed in color) Qualitative comparison on the domain conversion. Detailed structure in body region is lost with SimGAN, but reproduced with our model.

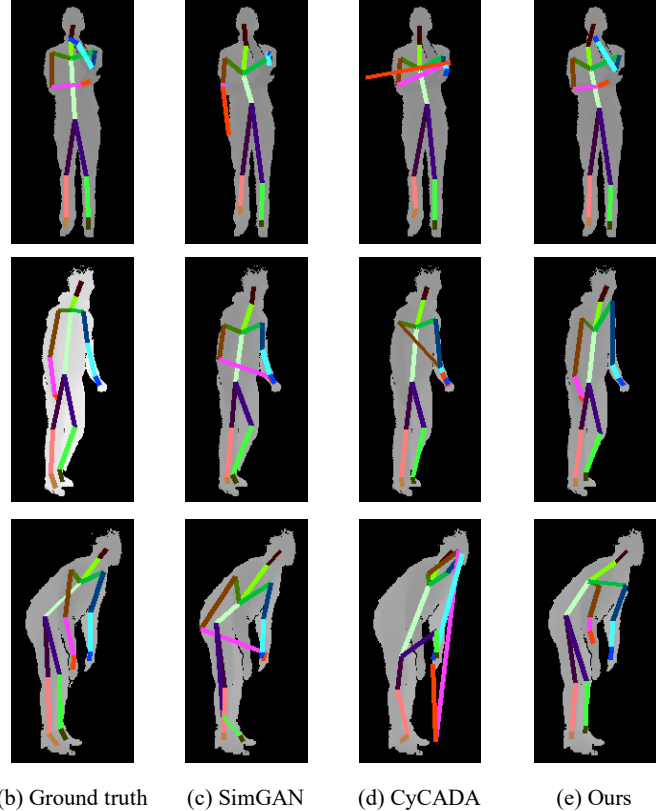(a) Input   (b) Ground truth   (c) SimGAN   (d) CyCADA   (e) Ours

Figure 9. (best viewed in color) Qualitative results of human-pose estimation. Due to the lack of detailed depth structure as seen in Fig. 8, SimGAN and CyCADA often fail to estimate joints with self-occlusion.

difference contributed to the prediction quality difference shown in Figure 9.

In the ablation study, we compared our full model with the following four different variations (see Table 6).

CycleGAN+L_{fc} does not divide z_s and z_t into the two components, but applied L_{fc} to z_s and z_t directly.

D-CycleGAN stands for disentangled CycleGAN, which divides z_s and z_t into the two components, but parameters of encoders and decoders are not shared and not using VAE at the calculation of L_{id}.

D-CycleGAN+VAE is a D-CycleGAN with L_{KL} and the resampling trick of VAE at the calculation of L_{id}.

PS-AEs stands for Partially-shared Auto-Encoders, whose encoders and decoders partially shares parameters as described in 3.4, but not using VAE.

PS-VAEs stands for Partially-shared Variational Auto-Encoders and this is the full model of the proposed method.

D-CycleGAN had actually performed the second best result and D-CycleGAN+VAE and PS-AEs did not work well.

First, as UNIT[19] does,[3] it seems to be difficult to use VAE with CycleGAN without sharing weights between the encoder-decoder models. After combining all these modifications, the full model of the proposed method outperformed any other methods with a large margin.

5. Conclusion

In this paper, we proposed a novel approach for unsupervised domain adaptation with target shift. Our approach generates pseudo-feature pairs (with identical labels) to obtain an encoder that aligns target domain samples into the same locations as source domain samples according to their label similarities. Target shift is a common setting in UDA tasks because target domain datasets are often not well organized as the source domain datasets in practice. To be robust against target shift, the method avoids using feature distribution matching but obtains a common feature space by pair-wise feature alignment. To prevent mis-alignment caused at adversarial training in image-space, a CycleGAN-based model was modified to divide features in domain-invariant and domain-specific components, to share weights

---

[3]Another neural network model that combines CycleGAN and VAE as the proposed model, but for image-to-image translation.

between two encoder-decoder parts, and to further disentangle features by the mechanism of a variational auto-encoder. We evaluated the model with digit classification tasks and achieved the best performance under the most of imbalanced situations. We also applied the method to a regression task of human-pose estimation and found that it outperformed the previous methods significantly.

References

[1] Z. Cao, M. Long, J. Wang, and M. I. Jordan. Partial transfer learning with selective adversarial networks. In *The IEEE Conference on Computer Vision and Pattern Recognition (CVPR)*. 2

[2] Z. Cao, L. Ma, M. Long, and J. Wang. Partial adversarial domain adaptation. In *The European Conference on Computer Vision (ECCV)*, 2018. 2, 5

[3] Z. Cao, K. You, M. Long, J. Wang, and Q. Yang. Learning to transfer examples for partial domain adaptation. In *The IEEE Conference on Computer Vision and Pattern Recognition (CVPR)*, 2019. 2

[4] CMU Graphics Lab. CMU graphics lab motion capture database. http://mocap.cs.cmu.edu/. (accessed on 11th-Nov-2019). 6

[5] M. Cordts, M. Omran, S. Ramos, T. Rehfeld, M. Enzweiler, R. Benenson, U. Franke, S. Roth, and B. Schiele. The cityscapes dataset for semantic urban scene understanding. In *Proceedings of the IEEE conference on computer vision and pattern recognition (CVPR)*, pages 3213–3223, 2016. 1

[6] Z. Deng, Y. Luo, and J. Zhu. Cluster alignment with a teacher for unsupervised domain adaptation. In *The IEEE International Conference on Computer Vision (ICCV)*, 2019. 1, 2, 3

[7] C. Doersch. Tutorial on variational autoencoders. 2016. 2

[8] M. Ghifary, W. B. Kleijn, and M. Zhang. Domain adaptive neural networks for object recognition. In *Pacific Rim international conference on artificial intelligence*, pages 898–904. Springer, 2014. 1, 2

[9] R. Girshick. Fast R-CNN. In *The IEEE International Conference on Computer Vision (ICCV)*. 5

[10] M. Gong, K. Zhang, T. Liu, D. Tao, C. Glymour, and B. Schölkopf. Domain adaptation with conditional transferable components. In *International Conference on Machine Learning (ICML)*, pages 2839–2848, 2016. 2

[11] J. Hoffman, E. Tzeng, T. Park, J.-Y. Zhu, P. Isola, K. Saenko, A. Efros, and T. Darrell. CyCADA: Cycle-consistent adversarial domain adaptation. 2018. 1, 2, 3, 6

[12] J. J. Hull. A database for handwritten text recognition research. *IEEE Transactions on Pattern Analysis and Machine Intelligence (PAMI)*, 16(5):550–554, 1994. 5

[13] H. Joo, H. Liu, L. Tan, L. Gui, B. Nabbe, I. Matthews, T. Kanade, S. Nobuhara, and Y. Sheikh. Panoptic studio: A massively multiview system for social motion capture. In *The IEEE International Conference on Computer Vision (ICCV)*, 2015. 6

[14] F. Kuhnke and J. Ostermann. Deep head pose estimation using synthetic images and partial adversarial domain adaption

[15] I. Laradji and R. Babanezhad. M-adda: Unsupervised domain adaptation with deep metric learning. 2018. 2

[16] Y. LeCun and C. Cortes. MNIST handwritten digit database. 2010. 5

[17] H.-Y. Lee, H.-Y. Tseng, J.-B. Huang, M. Singh, and M.-H. Yang. Diverse image-to-image translation via disentangled representations. In *The European Conference on Computer Vision (ECCV)*. 4

[18] A. H. Liu, Y.-C. Liu, Y.-Y. Yeh, and Y.-C. F. Wang. A unified feature disentangler for multi-domain image translation and manipulation. In *Advances in Neural Information Processing Systems 31*, pages 2590–2599. 2018. 1, 2, 5

[19] M.-Y. Liu, T. Breuel, and J. Kautz. Unsupervised image-to-image translation networks. In I. Guyon, U. V. Luxburg, S. Bengio, H. Wallach, R. Fergus, S. Vishwanathan, and R. Garnett, editors, *Advances in Neural Information Processing Systems 30 (NIPS*, pages 700–708. Curran Associates, Inc., 2017. 8

[20] Y. Liu, Z. Wang, H. Jin, and I. Wassell. Multi-task adversarial network for disentangled feature learning. In *In Proceedings of the IEEE Conference on Computer Vision and Pattern Recognition (CVPR)*, pages 3743–3751, 2018. 2, 5

[21] M. Long, Y. Cao, J. Wang, and M. I. Jordan. Learning transferable features with deep adaptation networks. In *Proceedings of the 32nd International Conference on International Conference on Machine Learning (ICML)*, pages 97–105. JMLR. org, 2015. 1, 2

[22] Y. Luo, L. Zheng, T. Guan, J. Yu, and Y. Yang. Taking a closer look at domain shift: Category-level adversaries for semantics consistent domain adaptation. In *The IEEE Conference on Computer Vision and Pattern Recognition (CVPR)*. 2

[23] L. v. d. Maaten and G. Hinton. Visualizing data using t-SNE. *Journal of Machine Learning Research*, 9(Nov):2579–2605, 2008. 7

[24] X. Mao, Q. Li, H. Xie, R. Y. Lau, Z. Wang, and S. Paul Smolley. Least squares generative adversarial networks. In *Proceedings of the IEEE International Conference on Computer Vision (ICCV)*, pages 2794–2802, 2017. 3

[25] T. Miyato, T. Kataoka, M. Koyama, and Y. Yoshida. Spectral normalization for generative adversarial networks. In *International Conference on Learning Representations*, 2018. 3

[26] J. G. Moreno-Torres, T. Raeder, R. Alaiz-RodríGuez, N. V. Chawla, and F. Herrera. A unifying view on dataset shift in classification. *Pattern Recognition*, 45(1):521–530, 2012. 2

[27] Y. Netzer, T. Wang, A. Coates, A. Bissacco, B. Wu, and A. Y. Ng. Reading digits in natural images with unsupervised feature learning. 2011. 5

[28] S. R. Richter, V. Vineet, S. Roth, and V. Koltun. Playing for data: Ground truth from computer games. In *European conference on computer vision (ECCV)*, pages 102–118. Springer, 2016. 1

[29] S. Roy, A. Siarohin, E. Sangineto, S. R. Bulo, N. Sebe, and E. Ricci. Unsupervised domain adaptation using feature-whitening and consensus loss. In *Proceedings of the IEEE*

Conference on Computer Vision and Pattern Recognition (CVPR), pages 9471–9480, 2019. 2, 6

[30] P. Russo, F. M. Carlucci, T. Tommasi, and B. Caputo. From source to target and back: Symmetric bi-directional adaptive gan. In *Proceedings of the IEEE Conference on Computer Vision and Pattern Recognition (CVPR)*, pages 8099–8108, 2018. 2, 3, 6

[31] K. Saito, Y. Ushiku, T. Harada, and K. Saenko. Adversarial dropout regularization. In *The International Conference on Learning Representations (ICLR)*, 2018. 1, 2

[32] K. Saito, K. Watanabe, Y. Ushiku, and T. Harada. Maximum classifier discrepancy for unsupervised domain adaptation. In *Proceedings of the IEEE Conference on Computer Vision and Pattern Recognition (CVPR)*, pages 3723–3732, 2018. 1, 2, 6

[33] A. Shrivastava, T. Pfister, O. Tuzel, J. Susskind, W. Wang, and R. Webb. Learning from simulated and unsupervised images through adversarial training. In *Proceedings of the IEEE conference on computer vision and pattern recognition (CVPR)*, pages 2107–2116, 2017. 2, 3, 5

[34] R. Shu, H. Bui, H. Narui, and S. Ermon. A DIRT-T approach to unsupervised domain adaptation. In *International Conference on Learning Representations (ICLR)*, 2018. 2

[35] P. Software. Poser pro 2014. https://www.renderosity.com/mod/bcs/poser-pro-2014/102000. (accessed on 10th-Nov-2019). 6

[36] E. Tzeng, J. Hoffman, K. Saenko, and T. Darrell. Adversarial discriminative domain adaptation. In *The IEEE Conference on Computer Vision and Pattern Recognition (CVPR)*, 2017. 1, 2, 5

[37] H. Yan, Y. Ding, P. Li, Q. Wang, Y. Xu, and W. Zuo. Mind the class weight bias: Weighted maximum mean discrepancy for unsupervised domain adaptation. In *The IEEE Conference on Computer Vision and Pattern Recognition (CVPR)*. 2

[38] J. Zhang, Z. Ding, W. Li, and P. Ogunbona. Importance weighted adversarial nets for partial domain adaptation. In *The IEEE Conference on Computer Vision and Pattern Recognition (CVPR)*. 2

[39] K. Zhang, B. Schölkopf, K. Muandet, and Z. Wang. Domain adaptation under target and conditional shift. In *International Conference on Machine Learning (ICML)*, pages 819–827, 2013. 2

[40] X. Zhang, Y. Wong, M. S. Kankanhalli, and W. Geng. Unsupervised domain adaptation for 3D human pose estimation. In *Proceedings of the 27th ACM International Conference on Multimedia*, 2019. 3

[41] J.-Y. Zhu, T. Park, P. Isola, and A. A. Efros. Unpaired image-to-image translation using cycle-consistent adversarial networks. In *The IEEE International Conference on Computer Vision (ICCV)*, 2017. 2, 3

A. Supplementary Material for Partially-Shared Variational Auto-encoders for Unsupervised Domain Adaptation with Target Shift

A.1. Hyper-parameters

As defined in Eq. (6) in the main paper,

The proposed method has five hyper-parameters of $\alpha, \beta, \gamma, \delta, \epsilon$. In each experiment, we set these hyper-parameters as listed in Table G.

A.2. Network structure

Table H shows the backbone architecture used in the digit classification task. We basically used the original backbone architecture for each comparative method if it exists. In the human pose estimation task, we used the same network architecture designed for this specific task because any other UDA methods have never tried it.

The detail of the backbone network architectures used in the tasks are shown in Table I, where ResBlock is defined in Table J. In addition to the input data size, they have difference in the architecture of M, which is a digit classifier or a human pose regressor. We also note that ResBlocks in the encoder and the decoder are removed in the task of ResBlock in MNIST→USPS. z and ζ_* are set to 64 and 96 channels in any of the experiments, respectively.

A.3. Data augmentation in the SVHN → MNIST task

In the SVHN → MNIST task, some conventional methods (UFDN, CyCADA) augmented training images in the MNIST dataset by inverting all pixel values by chance. The reported results of these methods and the proposed method are obtained with this augmentation.

A.4. Background subtraction for the target domain data in human pose estimation

The depth images in the CMU panoptic dataset contains cluttered background regions, which are diverse and essentially not related to human pose. These background regions are detected automatically in a pre-process. Since depth values in a background are always bigger than the foreground in nature, background images can be generated from by obtaining the maximum depth value at each pixel as long as the image data is given as a video captured by a fixed camera. For all images in the target domain dataset, we obtained its background image in this way and applied background subtraction in advance. We set a uniform pixel value to the detected background regions. After that, the detected foreground regions (i.e., human regions) were cropped with the aspect ratio of $2 : 1$ and resized to 256 channels $\times$ 128 pixels.

Table G. hyper-parameters used in the experiments.

	α	β	γ	δ	ϵ
digit classification	3	1	3	10	3
human pose estimation	5	10	3	20	3

Table H. Networks used in each method for digit classification. "original" indicated that the network is the same with that used in the original paper.

	digit classification
Source only	same as ADDA
ADDA	original
UFDN	original
PADA	same as ADDA
SimGAN	same as CyCADA
CyCADA	original
MCD	original
PS-VAEs	our digit network

Note that the uniform value of the background region is equal to that of CG images. In addition, the same cropping and resizing process were performed to CG images.

B. Joint distributions

We show all the distributions of joint positions in Figures J. Note that right hand can appear in the both sides of the image by chance because the direction of the human is not fixed.

Table I. Backbone network architecture of digit classification and human pose estimation.

The size of input x_*

	height	width	channel(s)
MNIST↔USPS	32	32	1
SVHN→MNIST	32	32	3
pose estimation	256	128	1

Encoder E_*

Input	$h \times w \times c$
Conv	$7 \times 7 \times 64$, refrectionpad 3
Parametrized ReLU	
Conv	$3 \times 3 \times 128$, pad 1, stride 2
Parametrized ReLU	
Conv	$3 \times 3 \times 256$, pad 1, stride 2
Parametrized ReLU	
ResBlock	256 channels
ResBlock	256 channels
ResBlock	256 channels
ResBlock	256 channels
(mu) Conv	$3 \times 3 \times 256$, pad 1
(logvar) Conv	$3 \times 3 \times 256$, pad 1
Output	$h/4 \times w/4 \times 256$

Decoder G_*

Input	$h/4 \times w/4 \times 256$
ResBlock	256 channels
ResBlock	256 channels
ResBlock	256 channels
ResBlock	256 channels
Upsampling	$2 \times 2 \times 256$
Conv	$3 \times 3 \times 128$, pad 1
Parametrized ReLU	
Upsampling	$2 \times 2 \times 128$
Conv	$3 \times 3 \times 64$, pad 1
Parametrized ReLU	
Conv	$7 \times 7 \times c$, reflectionpad 3
Output	$h \times w \times c$

Classifier M (for digit classification)

Input	8×8×64 channels
Flatten	4096
Parametrized ReLU	
Dropout	50%
Full connection	10
Output	10

Regresser M (for human pose estimation)

Regressor M	
Input	8×8×64 channels
ResBlock	64 channels
ResBlock	64 channels
ResBlock	64 channels
ResBlock	64 channels
Upsampling	$2 \times 2 \times 64$
Conv	$3 \times 3 \times 32$, pad 1
Parametrized ReLU	
Upsampling	$2 \times 2 \times 32$
Conv	$3 \times 3 \times 16$, pad 1
Parametrized ReLU	
Conv	$7 \times 7 \times 18$, reflectionpad 3
Output	$h \times w \times 18$

Discriminator D_*

Input	$h \times w \times c$
Conv	$4 \times 4 \times 64$, pad 2, stride 2
Spectral norm	
Parametrized ReLU	
Conv	$4 \times 4 \times 128$, pad 2, stride 2
Spectral norm	
Parametrized ReLU	
Conv	$4 \times 4 \times 256$, pad 2, stride 2
Spectral norm	
Parametrized ReLU	
Conv	$4 \times 4 \times 512$, pad 2, stride 2
Spectral norm	
Parametrized ReLU	
Conv	$4 \times 4 \times 512\times$, pad 2
Spectral norm	
Parametrized ReLU	
Conv	$4 \times 4 \times 1$, pad 2
Output	$(h/16 + 4) \times (w/16 + 4)$

Table J. Definition of ResBlock.

Input	$h \times w \times c_{in}$
Conv	$3 \times 3 \times c_{in}$, pad 1
Parametrized ReLU	
Conv	$3 \times 3 \times c_{in}$, pad 1
Parametrized ReLU	
Output	$h \times w \times c_{out}$

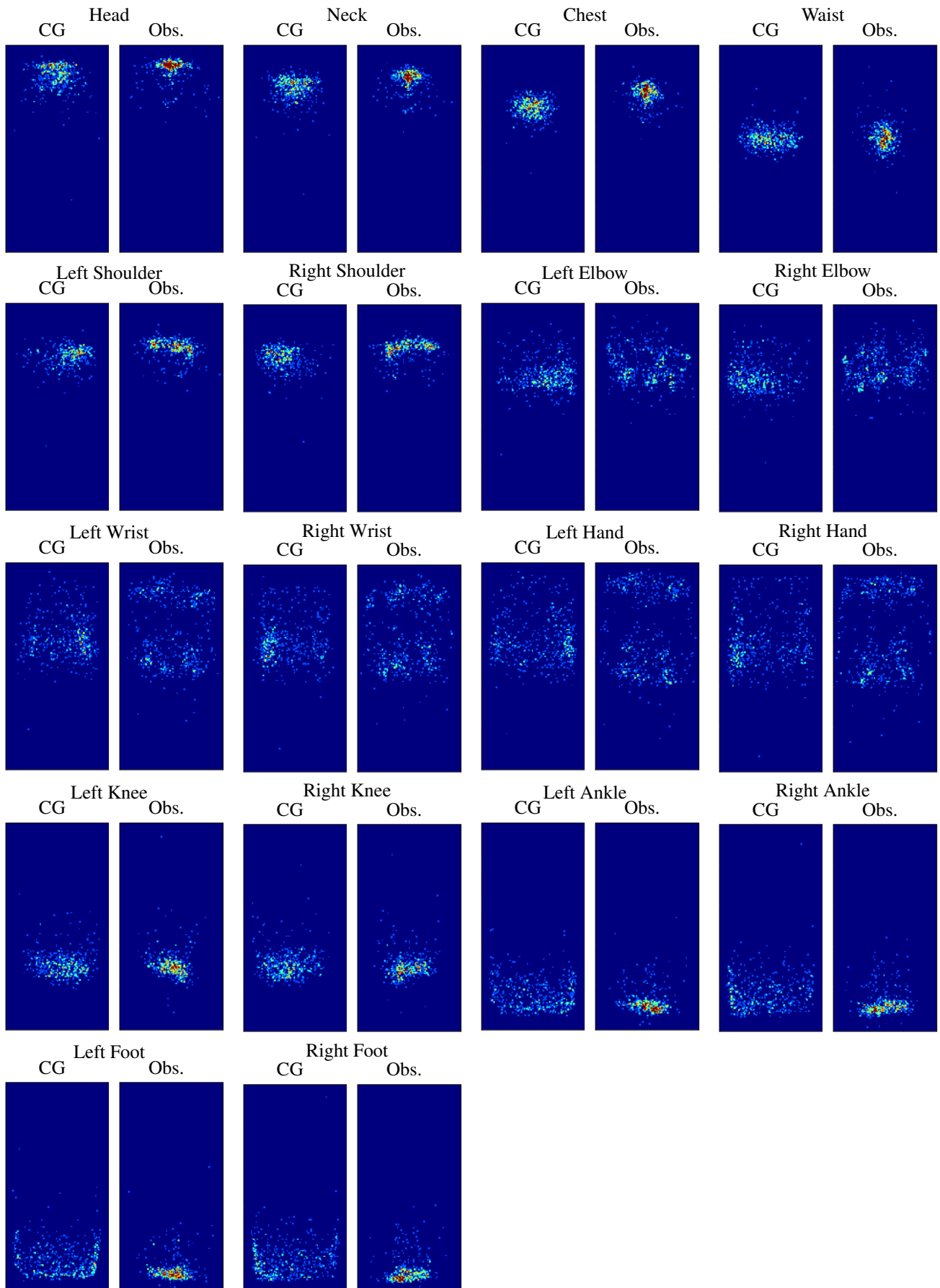| Error less than 10px.	Head	Neck	Chest	Waist	Shoulder	Elbow	Wrists	Hands	Knees	Ankles	Foots	Avg.
Source only	0.4	3.6	1.2	0.4	1.0	2.8	1.0	2.8	1.0	2.6	2.3	1.8
MCD	4.6	7.0	0.2	0.6	1.4	0.2	0.3	0.9	0.4	21.0	16.6	5.3
SimGAN	**90.2**	68.0	10.8	22.6	38.8	26.3	28.5	33.6	35.9	52.5	52.8	40.4
CyCADA	90.0	69.0	15.4	28.2	39.5	27.3	31.3	32.5	35.4	54.4	53.2	41.0
PS-VAEs(Ours)	89.4	**84.6**	**21.4**	**43.4**	**51.7**	**54.4**	**49.4**	**43.9**	**45.6**	**74.5**	**74.0**	**57.0**

Figure J. Difference in pose distribution between Observed images and CG images.